

Supporting Information

Permetylation Introduces Destructive Quantum Interference in Saturated Silanes

Marc H. Garner^{1†}, Haixing Li^{2‡†}, Madhav Neupane^{3‡}, Qi Zou³, Taifeng Liu^{3, 4}, Timothy A. Su³, Zhichun Shangguan^{4▽}, Daniel W. Paley³, Fay Ng³, Shengxiong Xiao⁴, Colin Nuckolls^{3*}, Latha Venkataraman^{2, 3*}, Gemma C. Solomon^{1*}

¹ Nano-Science Center and Department of Chemistry, University of Copenhagen, Universitetsparken 5, 2100 Copenhagen Ø, Denmark

² Department of Applied Physics and Applied Mathematics, Columbia University, New York, New York 10027, United States

³ Department of Chemistry, Columbia University, New York, New York 10027, United States

⁴ The Education Ministry Key Lab of Resource Chemistry, Shanghai Key Laboratory of Rare Earth Functional Materials, Optoelectronic Nano Materials and Devices Institute, Department of Chemistry, Shanghai Normal University, Shanghai 200234, China

†These authors contributed equally.

Table of contents

A. Conformational analysis	S2
B. Transmission of linear and 222 compounds under torsion	S15
C. Synthetic procedures	S17
D. NMR characterization of the compounds	S19
E. Crystal structure of trans <i>cyclo-Si6(Me)</i>	S22
F. Molecular orbitals	S23
G. Transmission of linear molecules	S26
References	S27

A. Conformational Analysis

In this section follows a brief conformational analysis of the cyclic compounds described in the manuscript. The cyclic compounds have well-known large conformational freedom, which we need to consider in relation to the single-molecule conductance.¹⁻² The bicyclo[2.2.2] compounds have very little conformational freedom as discussed in previous work, and will only be discussed briefly here.³⁻⁴

During a single-molecule break-junction experiment it is possible that different conformations are sampled. The purpose of this conformational analysis is to find representative conformations for which we analyze the transmission. Due to the nature of a pulling experiment, we need to consider both the conformation energies and the molecular length, as the molecule is likely to extend into long conformations if there are no large intramolecular barriers.

A.1 Conformational analysis of six-membered rings

In the analysis, we consider the conformational space of the six-membered rings and the threefold torsion around each methylthiomethyl linker, which can be arbitrarily defined by one of the C/Si–C/Si–CH₂–S dihedral angles. The terminal methyl group is always considered to be in transoid position (C/Si–CH₂–S–CH₃ dihedral angle = ~180°) when we calculate the conformation energy. The conformational space is the same for the *trans*-isomers of all four cyclohexyl compounds, and is shown diagrammatically in Figure S1. In a disubstituted six-membered ring there is the well-known chair conformation which will have both substituents in either equatorial or axial position, and there are two types of twist-boat conformations: in 3,6-twist both substituents are in equivalent positions, and in 1,4-twist one substituent is in the axial-like flagpole and the other substituent is in the equatorial-like bowsprit position (in accordance with the IUPAC boat terminology).

All molecules were optimized in vacuum to 5 meV/Å using PBE functional with a DZP basis set for all atoms as implemented in ASE and GPAW.⁵⁻⁸ We also carried out the analysis at the M06-2X/6-311G(d) level of theory as implemented in Gaussian09.⁹⁻¹⁰ The analysis is focused around the two experimental systems **cyclo-C6(H)** and **cyclo-Si6(Me)**, but the analysis is also carried out for the equivalent conformations of **cyclo-C6(Me)** and **cyclo-Si6(H)**.

All optimized structure files are uploaded as supporting data in xyz-format.

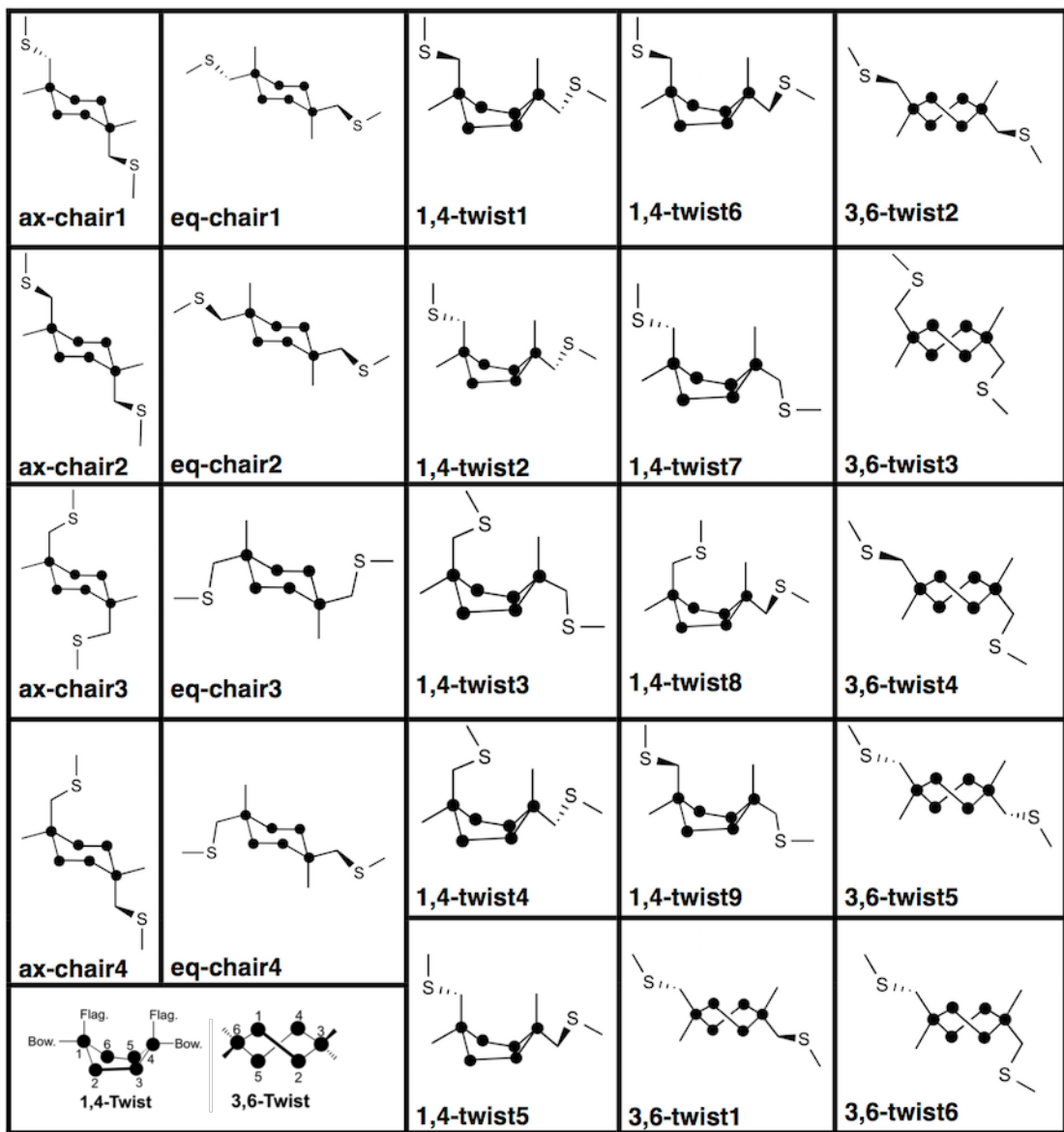


Figure S1. Overview of the conformational space considered for *cyclo-Si6* and *cyclo-C6*.

Listed in Table S1, *cyclo-C6(H)* has, as one would expect, predominantly conformations with the bulky linkers in the favourable equatorial configurations of the chair conformations, and only equatorial chairs needs to be considered in our analysis. While these are near-degenerate, it is worth noting that eq-chair1 is slightly longer than eq-chair2, which again is slightly longer than eq-chair3 and 4. The energies are quite similar at the PBE/DZP and M06-2X/6-311G(d) levels of theory.

Listed in Table S2, the distribution of *cyclo-C6(Me)* is very similar. Eq-chair1 is the most stable conformation at both the PBE/DZP and M06-2X/6-311G(d) levels of theory, and long equatorial chairs are expected to dominate in a potential experiment.

Table S1. Conformations *Cyclo-C6(H)* given in eV.

Conformer	E(PBE/DZP)	E(M06-2X/6-311G(d))
Ax-chair1	0.17	0.13
Ax-chair2	0.17	0.14
Ax-chair3	0.31	0.36
Ax-chair4	0.24	0.24
Eq-chair1	0.00	0.00
Eq-chair2	0.00	0.01
Eq-chair3	0.04	0.05
Eq-chair4	0.03	0.03
3,6-twist1	0.28	0.32
3,6-twist2	0.30	0.27
3,6-twist3	0.30	0.31
3,6-twist4	0.30	0.29
3,6-twist5	0.27	0.27
3,6-twist6	0.30	0.30
1,4-twist1	0.33	0.30
1,4-twist2	0.33	0.33
1,4-twist3	0.31	0.31
1,4-twist4	0.38	0.39
1,4-twist5	0.34	0.31
1,4-twist6	0.34	0.30
1,4-twist7	0.34	0.34
1,4-twist8	0.39	0.39
1,4-twist9	0.35	0.32

Table S2. Conformations *Cyclo-C6(Me)* given in eV.

Conformer	E(PBE/DZP)	E(M06-2X/6-311G(d))
Ax-chair1	0.10	0.07
Ax-chair2	0.11	0.10
Ax-chair3	0.46	0.54
Ax-chair4	0.25	0.25
Eq-chair1	0.00	0.00
Eq-chair2	0.02	0.04
Eq-chair3	0.38	0.32
Eq-chair4	0.12	0.18
3,6-twist1	0.29	0.21
3,6-twist2	0.20	0.20
3,6-twist3	0.48	0.45
3,6-twist4	0.33	0.33
3,6-twist5	0.38	0.22
3,6-twist6	0.43	0.35
1,4-twist1	0.27	0.22
1,4-twist2	0.30	0.26
1,4-twist3	0.58	0.65
1,4-twist4	0.49	0.55
1,4-twist5	0.21	0.15
1,4-twist6	0.21	0.19
1,4-twist7	0.44	0.41
1,4-twist8	0.43	0.48
1,4-twist9	0.39	0.34

Listed in Table S3, the conformation distribution of **cyclo-Si6(H)** reveals that a range of conformations may be accessible during a potential junction experiment. At the M06-2X/6-311G(d) level of theory the short axial chairs are found to be the most stable. These are likely to be pulled into longer conformations.

Table S3. Conformations *Cyclo-Si6(H)* given in eV.

Conformer	E(PBE/DZP)	E(M06-2X/6-311G(d))
Ax-chair1	0.02	0.03
Ax-chair2	0.02	0.03
Ax-chair3	0.00	0.00
Ax-chair4	0.02	0.03
Eq-chair1	0.03	0.12
Eq-chair2	0.03	0.13
Eq-chair3	0.03	0.11
Eq-chair4	0.04	0.12
3,6-twist1	0.10	0.12
3,6-twist2	0.09	0.15
3,6-twist3	0.10	0.13
3,6-twist4	0.09	0.13
3,6-twist5	0.13	0.17
3,6-twist6	0.11	0.11
1,4-twist1	0.10	0.12
1,4-twist2	0.13	0.11
1,4-twist3	0.11	0.10
1,4-twist4	0.08	0.08
1,4-twist5	0.11	0.12
1,4-twist6	0.08	0.10
1,4-twist7	0.13	0.15
1,4-twist8	0.07	0.08
1,4-twist9	0.10	0.11

The energy distribution of **cyclo-Si6(Me)**, listed in Table S4, shows that an even wider range of conformations may be accessed during the pulling experiment. The most stable conformations at both levels of theory are the short ax-chair3 and ax-chair4 conformations, while a range of near-degenerate equatorial chair and twist conformations exist which are much longer. These are likely to be accessed as the molecule extends to its full length during the pull if the internal barriers are not high. The transition states (TS) between conformations generally fall into two categories. From the short axial-chair the molecule must go through a half-chair TS (Fig. S2) into a twist conformation, and from there again through another half-chair TS into an equatorial chair conformation. Twist conformations interconvert through the well-known boat TS (Fig. S2).^{1-2, 11-12}

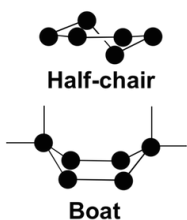


Figure S2. Half-chair and boat transition-states of **cyclo-Si(Me)**.

We estimate the internal barriers between conformations using the nudged elastic band method¹³⁻¹⁵ as implemented in ASE and GPAW.⁶⁻⁸ Barriers were calculated at the PBE/DZP level of theory. All calculated barriers are listed in Table S5 along with the change of sulfur-sulfur length, and the results are summarized in Figure S3.

We first note that, as expected, the boat TSs are all small barriers and will interconvert rapidly at room temperature. The linker (sulfur) torsion TS for all conformations is also found to be a small barrier of around 0.1 eV (~9.6 kJ/mol, ~2.3 kcal/mol). Barriers from the axial-chair going into the 1,4-twist and longer 3,6-twist conformations are relatively small (below 0.2 eV, (~19 kJ/mol, ~4.6 kcal/mol), and may go through small barriers into 1,4-twist before going into the long 3,6-twist and eq-chair conformations. The barrier from 3,6-twist into the long equatorial-chairs are below 0.15 eV (~14 kJ/mol, ~3.5 kcal/mol). With multiple ways through the conformational space over small energy barriers, it is possible that multiple conformations are sampled during the timescale of the experiment before the longest conformation(s) are sampled at the end. The crystal structure of the molecule (Fig. S8) is the eq-chair1 conformation, which is the longest conformation, and the one with second lowest energy in the calculation (third lowest energy with the M06-2X functional). Therefore we focus on the eq-chair1 conformation as a representative structure of the molecule.

Table S4. Conformations *Cyclo-Si6(Me)* given in eV.

Conformer	E(PBE/DZP)	E(M06-2X/6-311G(d))
Ax-chair1	0.08	0.09
Ax-chair2	0.08	0.08
Ax-chair3	0.00	0.00
Ax-chair4	0.07	0.04
Eq-chair1	0.05	0.08
Eq-chair2	0.06	0.09
Eq-chair3	0.05	0.12
Eq-chair4	0.06	0.09
3,6-twist1	0.12	0.14
3,6-twist2	0.07	0.08
3,6-twist3	0.09	0.12
3,6-twist4	0.07	0.10
3,6-twist5	0.18	0.21
3,6-twist6	0.14	0.16
1,4-twist1	0.09	0.10
1,4-twist2	0.11	0.12
1,4-twist3	0.08	0.10
1,4-twist4	0.08	0.08
1,4-twist5	0.09	0.09
1,4-twist6	0.08	0.09
1,4-twist7	0.13	0.14
1,4-twist8	0.05	0.14
1,4-twist9	0.12	0.14

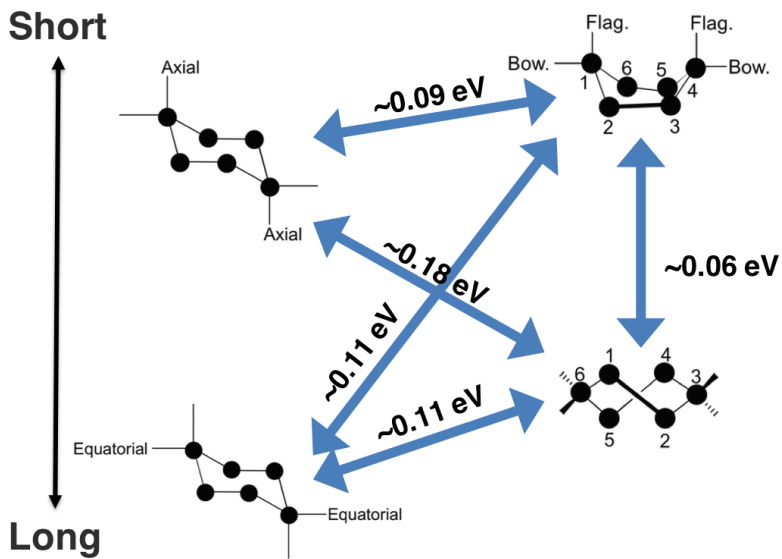


Figure S3. Schematic illustration of approximate barrier heights between conformations of *cyclo-Si6(Me)*. The four conformations are sorted by increasing molecular length from top to bottom.

Table S5: Internal Barriers of Cyclo-Si6(Me) towards the longer conformation (ΔE^\rightarrow) and change of sulfur-sulfur length.

1,4-twist \rightarrow ax-chair		ΔE^\rightarrow (eV)
Conformers	$\Delta(S-S)$ (\AA)	
1,4-twist1 \rightarrow ax-chair1	1.2	0.08
1,4-twist5 \rightarrow ax-chair1	0.6	0.11
1,4-twist2 \rightarrow ax-chair2	1.0	0.08
1,4-twist6 \rightarrow ax-chair2	0.9	0.09
ax-chair3 \rightarrow 1,4-twist3	0.6	0.15
1,4-twist4 \rightarrow ax-chair4	0.9	0.06
1,4-twist8 \rightarrow ax-chair4	1.4	0.09

1,4-twist \rightarrow eq-chair		
Conformers	$\Delta(S-S)$ (\AA)	ΔE^\rightarrow (eV)
1,4-twist1 \rightarrow eq-chair1	1.8	0.15
1,4-twist5 \rightarrow eq-chair1	2.4	0.04
1,4-twist2 \rightarrow eq-chair2	2.3	0.06
1,4-twist6 \rightarrow eq-chair2	3.0	0.11
1,4-twist3 \rightarrow eq-chair3	1.8	0.10
1,4-twist4 \rightarrow eq-chair4	2.3	0.14
1,4-twist8 \rightarrow eq-chair4	2.9	0.14

1,4-twist \rightarrow 3,6-twist		
Conformers	$\Delta(S-S)$ (Å)	ΔE^\rightarrow (eV)
1,4-twist1 \rightarrow 3,6-twist1	1.4	0.07
1,4-twist5 \rightarrow 3,6-twist1	2.0	0.05
1,4-twist2 \rightarrow 3,6-twist2	1.9	0.03
1,4-twist3 \rightarrow 3,6-twist3	0.6	0.06
1,4-twist4 \rightarrow 3,6-twist4	1.8	0.05
1,4-twist6 \rightarrow 3,6-twist5	1.8	0.10
1,4-twist8 \rightarrow 3,6-twist6	2.0	0.09

ax-chair \rightarrow 3,6-twist		
Conformers	$\Delta(S-S)$ (Å)	ΔE^\rightarrow (eV)
ax-chair1 \rightarrow 3,6-twist1	0.8	0.16
ax-chair2 \rightarrow 3,6-twist2	1.0	0.19
ax-chair3 \rightarrow 3,6-twist3	1.2	0.20
ax-chair4 \rightarrow 3,6-twist4	0.9	0.17

3,6-twist \rightarrow eq-chair		
Conformers	$\Delta(S-S)$ (Å)	ΔE^\rightarrow (eV)
3,6-twist1 \rightarrow eq-chair1	0.4	0.04
3,6-twist2 \rightarrow eq-chair2	0.3	0.11
3,6-twist3 \rightarrow eq-chair3	1.3	0.14
3,6-twist4 \rightarrow eq-chair4	0.5	0.13

Sulfur torsion		
Conformers	$\Delta(S-S)$ (Å)	ΔE^\rightarrow (eV)
ax-chair2 \rightarrow ax-chair1	0.4	0.11
ax-chair3 \rightarrow ax-chair4	1.1	0.09
eq-chair2 \rightarrow eq-chair1	0.3	0.11
eq-chair3 \rightarrow eq-chair4	0.2	0.07
1,4-twist2 \rightarrow 1,4-twist5	0.2	0.12
1,4-twist3 \rightarrow 1,4-twist8	0.9	—
1,4-twist3 \rightarrow 1,4-twist9	1.1	0.08
1,4-twist6 \rightarrow 1,4-twist5	0.1	0.11
1,4-twist8 \rightarrow 1,4-twist4	0.5	0.14
3,6-twist2 \rightarrow 3,6-twist1	0.3	0.14
3,6-twist3 \rightarrow 3,6-twist4	0.9	0.12

Here follows in Figure S4, the transmission of other conformations of **cyclo-C6(H)** and **cyclo-Si6(Me)**, which are not discussed in the manuscript. In **cyclo-C6(H)**, the transmission of the slightly shorter equatorial chairs is lower than that of eq-chair1, which was shown in the manuscript. Particularly eq-chair2 has lower transmission, and it is clear that the transmission has conformational dependence. This low transmission (of eq-chair2) is however not mirrored in the experimental conductance, and it may be that this conformation is not often sampled experimentally, possibly because eq-chair1 is longer and therefore more likely to be sampled during the pull.

For **cyclo-Si6(Me)** a much wider range of conformations may be sampled during the experiment. While eq-chair2 has somewhat high transmission, most conformations have fairly low transmission, similar to that of eq-chair1 which we showed in the manuscript. The long conformations (albeit shorter than eq-chair) eq-chair3 and 3,6-twist2 have sharp antiresonances, evident of σ -interference. The shorter ax-chair conformations and 1,4-twist6 have low transmission but not a clear antiresonance. This is possibly due to through-space interactions in these short structures, which may mask an antiresonance in the transmission. To summarize, most conformations seem to have low transmission, and it is likely that some of these are sampled during the pull in the STM-BJ experiments.

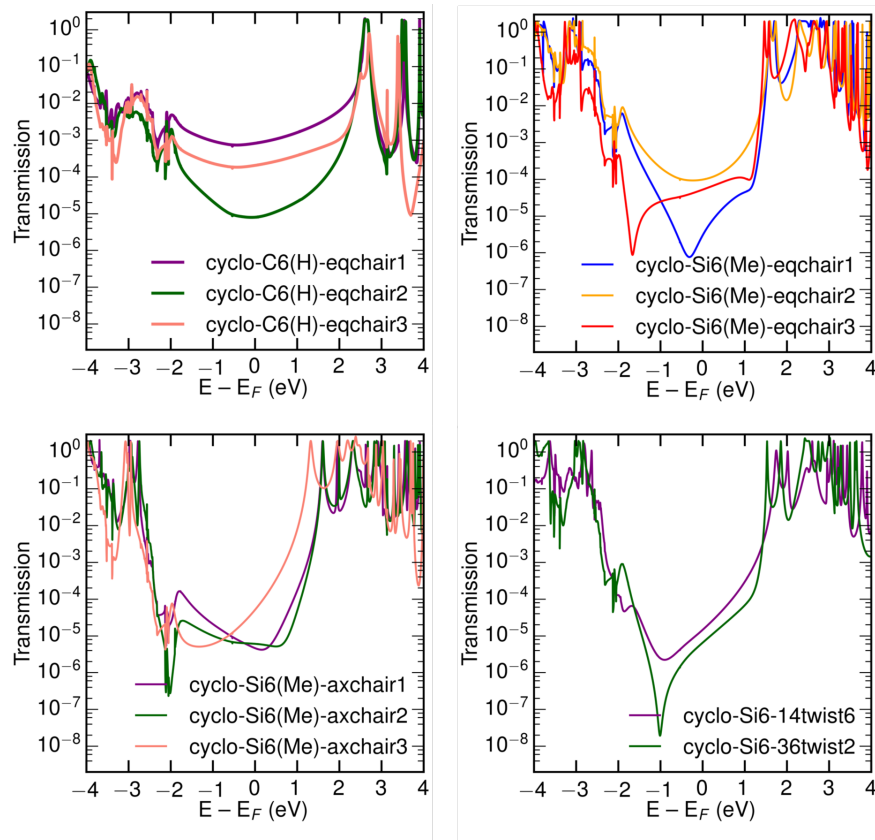


Figure S4. Transmission of various **cyclo-C6(H)** and **cyclo-Si6(Me)** conformations.

A.2 Conformation analysis of bicyclo[2.2.2] compounds

The conformational change in the bicyclo[2.2.2] compounds is limited due to the rigid cage, which we have described in previous work for Si222(Me).³⁻⁴ Considering the freedom around the two C/Si—C/Si—CH₂—S dihedral angles there are three different conformations which are shown in Figure S5.

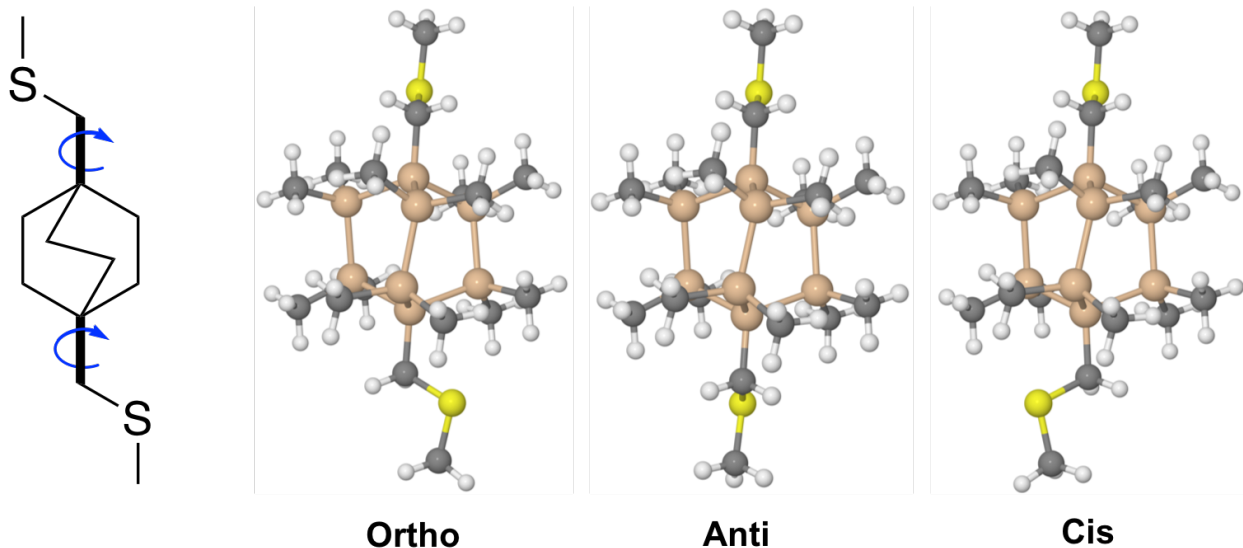


Figure S5. Left: Schematic of the conformational sampling around the linker axis of bicyclo[2.2.2] compounds. Right: Optimized structures of the three distinct conformations of Si222(Me).

Listed in Table S6 and S7, at both the PBE/DZP and M06-2X/6-311G(d) levels of theory, the three conformations are near-degenerate for all four bicyclic compounds.

Table S6. Energy of optimized conformations of bicyclo[2.2.2] compounds given in eV. Calculated at the PBE/DZP level of theory.

	C222(H)	C222(Me)	Si222(H)	Si222(Me)
Anti	0.01	0.02	0.01	0.01
Cis	0.00	0.01	0.00	0.01
Ortho	0.00	0.00	0.00	0.00

Table S7. Energy of optimized conformations of bicyclo[2.2.2] compounds given in eV. Calculated at the M06-2X 6-311G(d) level of theory.

	C222(H)	C222(Me)	Si222(H)	Si222(Me)
Anti	0.01	0.02	0.02	0.01
Cis	0.00	0.00	0.00	0.00
Ortho	0.00	0.00	*	0.00

* Optimization did not converge.

A.3 Comparison of structural parameters

In **Table S8** some representative structural parameters, as designated in **Scheme S1**, are shown for **cyclo-Si6(H)**, **cyclo-Si6(Me)**, **Si222(H)**, **Si222(Me)**, **cyclo-C6(H)**, **cyclo-C6(Me)**, **C222(H)** and **C222(Me)**. We include a central bond length (L), a central bond angle (A), and a central dihedral angle (D). These are taken from the relaxed junction structures. Some parameters are present in two places but are identical by symmetry; in the junction structure this can deviate a bit and we take the average value in such cases.

As expected the bond angles are larger in the permethylated molecules due to the bulkier methyl substituents. Bond angles are very similar, and differ mainly between the cyclic and bicyclic species as the latter is more constrained. Finally, the dihedral angles, which are known to be important for the transmission, differ up to 12° between the methylated and non-methylated molecules in the PBE-optimized junction structures.

We have taken the same parameters from the structures optimized at the M06-2X/6-311G(d) level of theory. Although there are some minor differences in the structures, the same result emerges. As we shall explore in the following section, this small difference in the angles does not appear to make a big difference in the transmission.

Scheme S1. Designation of Selected Structural Parameters.

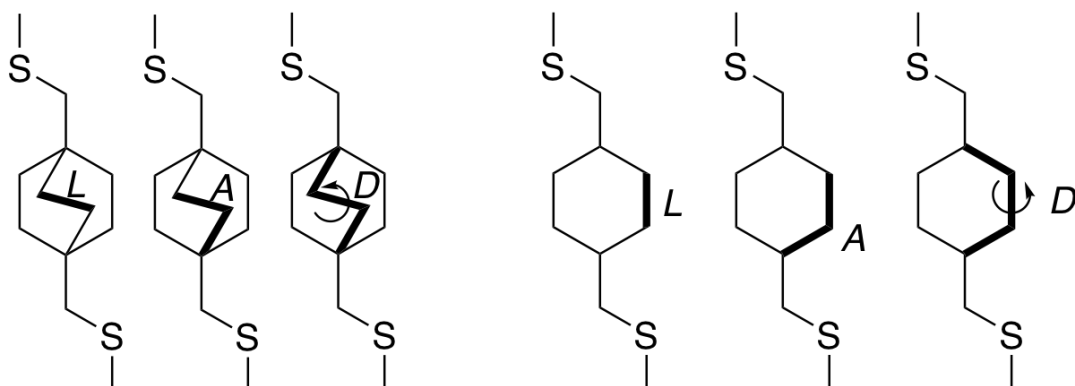


Table S8. Representative structural parameters (see **Scheme S1**). For calculations with PBE the parameter are taken from the optimized junction structures, for calculations with M06-2X the parameters are taken from the optimized vacuum structures.

Molecule	PBE/DZP (GPAW)			M06-2X/6-311G(d) (Gaussian09)		
	L (Å)	A (°)	D (°)	L (Å)	A (°)	D (°)
cyclo-Si6(H)	2.36	110.7	58.1	2.34	111.5	59.1
cyclo-Si6(Me)	2.38	112.6	54.0	2.35	114.5	51.2
Si222(H)	2.37	109.3	29.8	2.35	108.3	29.2
Si222(Me)	2.39	109.6	17.0	2.35	108.8	19.2
cyclo-C6(H)	1.54	112.0	55.5	1.53	112.1	56.1
cyclo-C6(Me)	1.63	114.2	47.6	1.60	114.2	47.9
C222(H)	1.56	110.3	13.8	1.55	109.8	18.5
C222(Me)	1.63	108.2	13.2	1.61	108.3	13.9

B. Transmission of Linear and 222 Compounds under Torsion

Here follows a brief examination of the dihedral angle dependence of the transmission through permethylated and non-permethylated silanes and alkanes. We and other have previously examined this structure-property relation for permethylated silanes and non-methylated alkanes.^{4, 16} In the light of the results presented in the manuscript, we here revisit this relation.

The following calculations were carried out as described in the manuscript using GPAW¹⁷ and ATK.¹⁸ In Figure S6, the transmission is calculated for the linear butane and tetrasilane species with methylthiomethyl linkers (**C6** and **Si4** as shown in the manuscript), where the central C-C-C-C or Si-Si-Si-Si dihedral angle is varied. The four atoms are kept fixed while other degrees of freedom are relaxed in the junction optimization. In both **C6(H)** and **Si4(H)** there is some degree of suppression at dihedral angles around 40-60°, but no clear antiresonance in the transmission. In the permethylated alkane **C6(Me)**, there is somewhat more suppression at dihedral angles 20-40° and antiresonance-like behaviour in the transmission. In the permethylated silane **Si4(Me)** a clear antiresonance and strong suppression is clear from 0-40°.

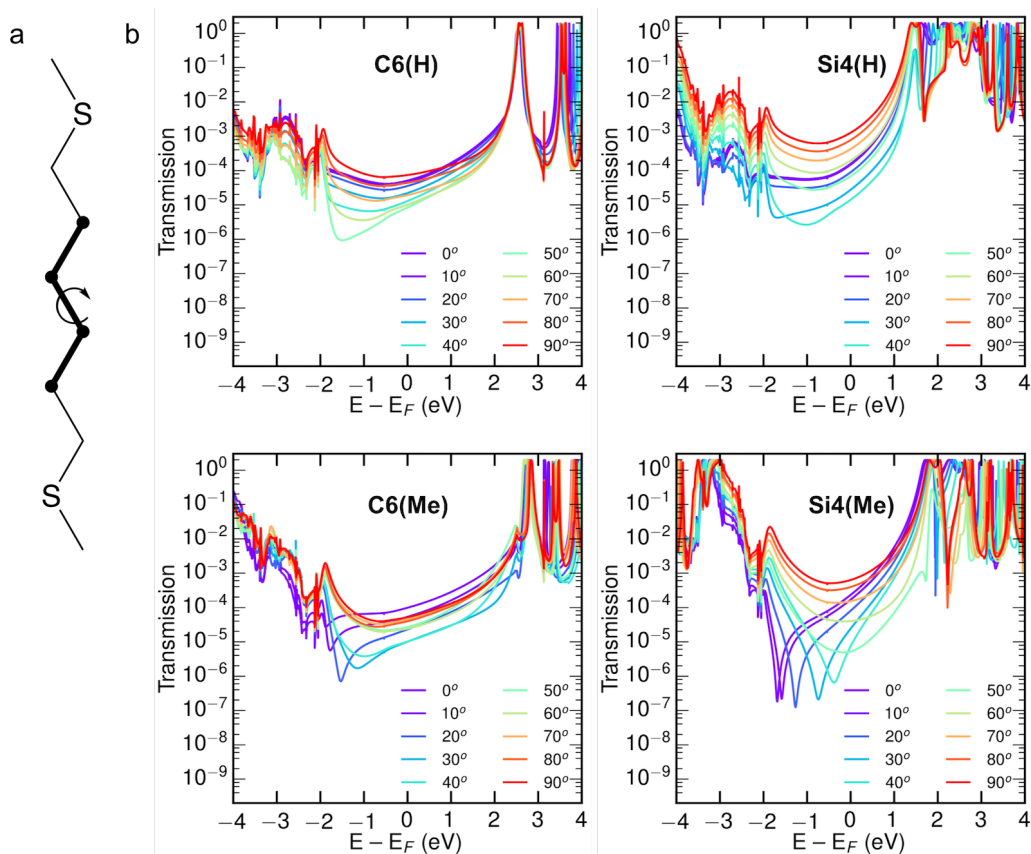


Figure S6. a) Torsion around the central dihedral angle of functionalized linear tetrasilane and butane. b) Transmission of non-methylated and permethylated linear tetrasilane and butane where the central dihedral angle is varied.

In Figure S7, the transmission for permethylated and non-methylated **C222** and **Si222** molecules is calculated under dihedral torsion. This torsion is made by rotating around the center of the molecule, i.e., the bridgehead-to-bridgehead Si-Si axis in order to maintain the overall structure of the bicyclic cage structure. The dihedral angle is defined as the Si-Si-Si-Si dihedral angle, equivalent to that for the linear systems. The junctions were not relaxed in these calculations.

In **C222(H)** and **Si222(H)**, there is almost no dependence of the transmission on the dihedral angle, and no clear suppression of the transmission. In the permethylated alkane **C222(Me)**, there is suppression at dihedral angles 0-20° and an antiresonance appears for the 0° and 10° cases. For the permethylated silane **Si222(Me)**, there is again a clear antiresonance and transmission suppression over a range of dihedral angles.

It is clear that in both the linear and cyclic alkanes and silanes, there cannot be full σ -interference in the non-methylated cases studied here. In some of the permethylated ones there are signatures of σ -interference, suggesting that there may be different alkanes where the effect is more pronounced. In permethylated silanes with constrained dihedral angles the σ -interference is clear, as we have seen in previous studies.^{3-4, 19}

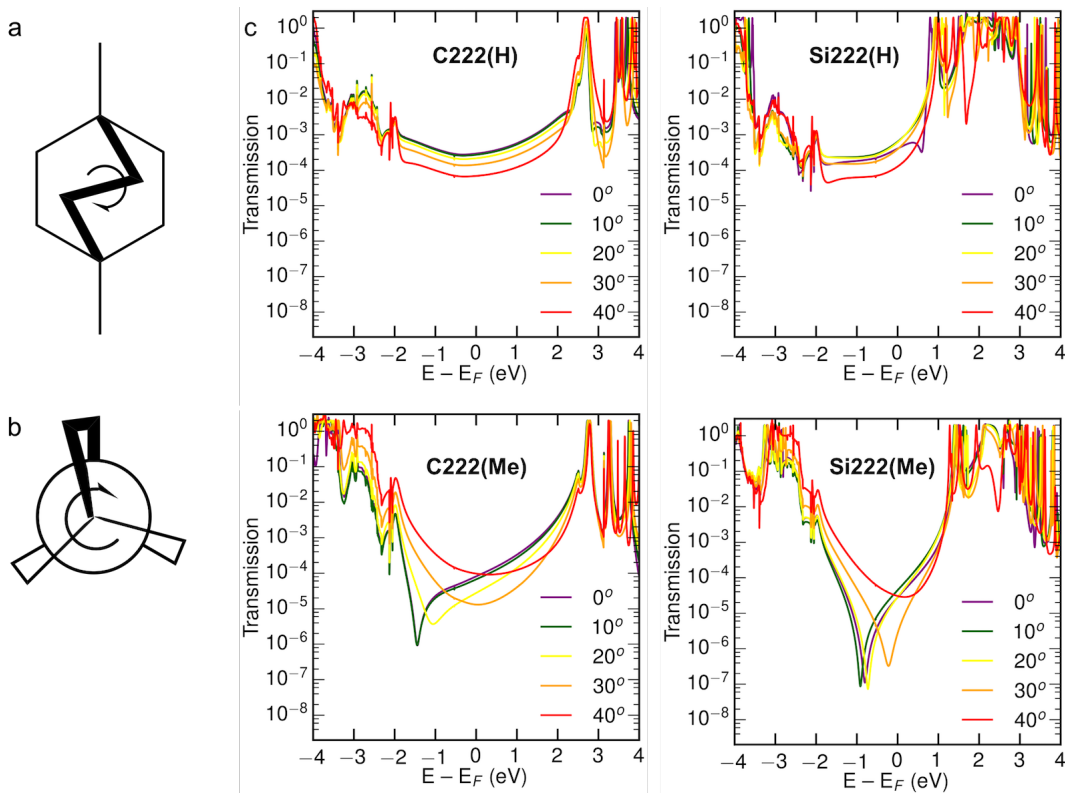


Figure S7. Transmission dependence of bicyclo[2.2.2] structure under torsion. a) The torsion angles are specified by the bridge Si-Si-Si-Si dihedral angle. b) The torsion is centered around the bridgehead-to-bridgehead axis to retain the symmetry of the molecule during the torsion. c) Transmission of non-methylated and permethylated **C222** and **Si222**.

C. Synthetic procedures

1. General Information

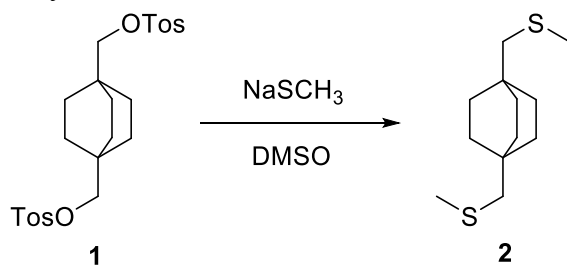
All reactions were performed in oven-dried or flame-dried round bottom flasks, unless otherwise noted. The flasks were fitted with Teflon magnetic stir bar, rubber septa and reactions were conducted under a positive pressure of nitrogen, unless otherwise noted. Anhydrous and anaerobic solvents were obtained from Schlenk manifold with purification columns packed with activated alumina and supported copper catalyst (Glass Contour, Irvine, CA). Automated flash chromatography was performed using a Teledyne Isco Combiflash R_f200 and Redisep R_f Silica/Alumina columns.

Materials. All chemicals were purchased from commercial sources and used without further purification unless otherwise specified. Compounds **1** and **3** were synthesized according to known procedures.²⁰⁻²¹ Compound **4** was purchased from AldrichCPR. All other compounds were purchased from Sigma Aldrich, Alfa Aesar, or Gelest.

Instrumentation. ¹H NMR and ¹³C NMR spectra in CDCl₃ were recorded on Brucker DRX400 (400 MHz) or a Bruker DMX500 (500 MHz) spectrometer. Chemical shifts for protons are reported in parts per million downfield from tetramethylsilane and are referenced to residual protium in the NMR solvents (CHCl₃: δ 7.26). Chemical shifts for carbon are reported in parts per million downfield from tetramethylsilane and are referenced to the carbon resonances of the solvent (CHCl₃: δ 77.0). Data are represented as follows: chemical shift, multiplicity (s = singlet, d = doublet, t = triplet, m = multiplet, br = broad), coupling constants in Hertz, and integration.

High-resolution mass spectrometry (HRMS) were recorded on a Waters XEVO G2-XS QTOF spectrometer with dichloromethane as solvent.

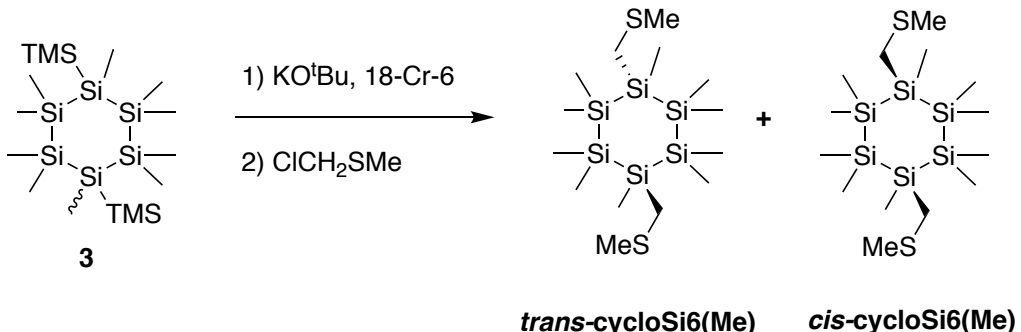
2. Synthesis



Synthesis of compound 2 (C222(H)).

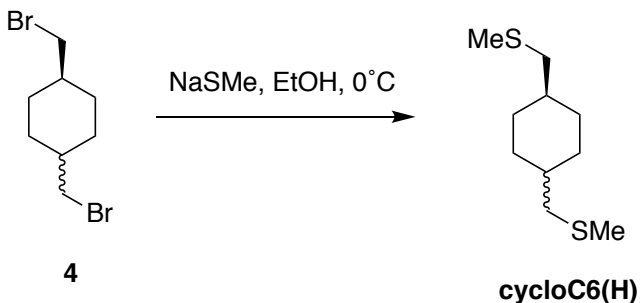
Under a nitrogen atmosphere, sodium thiomethoxide (56 mg, 0.80 mmol) was added to a solution of compound **1** (48 mg, 0.10 mmol) in DMSO (1.0 mL). The resultant suspension was heated to 80 °C. After stirring overnight, the solution was poured into a saturated NH₄Cl solution (10 mL), extracted with dichloromethane (10 mL × 3), and the combined organic layers were washed with brine solution (10.0 mL) and dried over anhydrous Na₂SO₄, filtered, and concentrated. The residue was purified by column chromatography (8 g Redisep R_f Neutral Alumina) using a gradient from 0% to 50% dichloromethane/hexanes to give the compound **2** (16 mg, 70%) as a white solid. ¹H NMR (400 MHz, CDCl₃) δ (ppm): 1.48 (s, 12H, -CH₂-), 2.09 (s, 6H, -SCH₃), 2.35 (s, 4H, -CH₂S-). ¹³C NMR (101 MHz, CDCl₃) δ (ppm): 18.14, 31.04, 33.05, 47.82. HRMS (ASAP+, m/z): [M]⁺ calcd for C₁₂H₂₂S₂, 230.1163; found, 230.1163.

Synthesis of *cyclo-Si6(Me)*



Compound 3 (0.341 mmol, 150 mg, 1.00 equiv.), potassium *tert*-butoxide (0.682 mmol, 76.5 mg, 2.00 equiv.), and 18-crown-6 (0.682 mmol, 180.3 mg, 2.00 equiv.) were added to a 25 mL Schlenk flask charged with a stir bar. 5 mL toluene was added to the solution and the mixture was stirred overnight. The reaction mixture was cooled to -78°C then cannula transferred to a separate 25 mL Schlenk flask charged with a stir bar and chloromethyl methyl sulfide (0.682 mmol, 65.9 mg, 2.00 equiv) dissolved in 5 mL toluene. The resulting solution was warmed to room temperature and stirred for 4 hours. The mixture was quenched with saturated ammonium chloride (2 mL), the organic and aqueous layers were separated, and the aqueous layer was extracted 3x with diethyl ether (10 mL each). The organic layers were washed with brine, dried over sodium sulfate, and concentrated *in vacuo* to yield a crude white semi-solid. The *trans* isomer was selectively crystallized from diethyl ether at -30°C . Single crystals suitable for single-crystal x-ray diffraction were grown from diethyl ether at -30°C . ^1H NMR (500 MHz, CDCl_3) δ 2.18 (s, 6H), 2.05 (s, 4H), 0.24 (s, 6H), 0.23 (s, 12H), 0.21 (s, 12H). ^{13}C NMR (101 MHz, CDCl_3) δ 21.90, 15.85, 1.83, -2.81, -3.33.

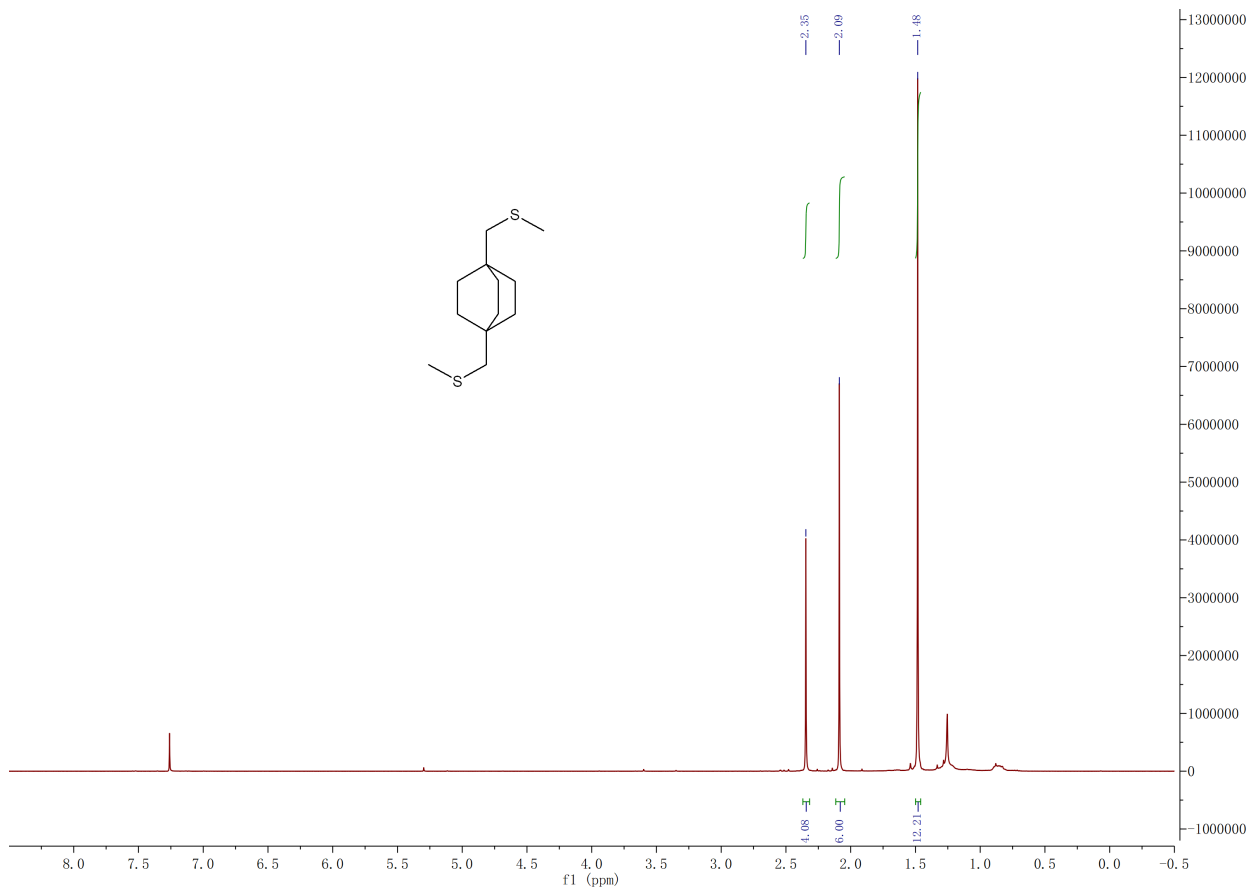
Synthesis of *cyclo-C6(H)*



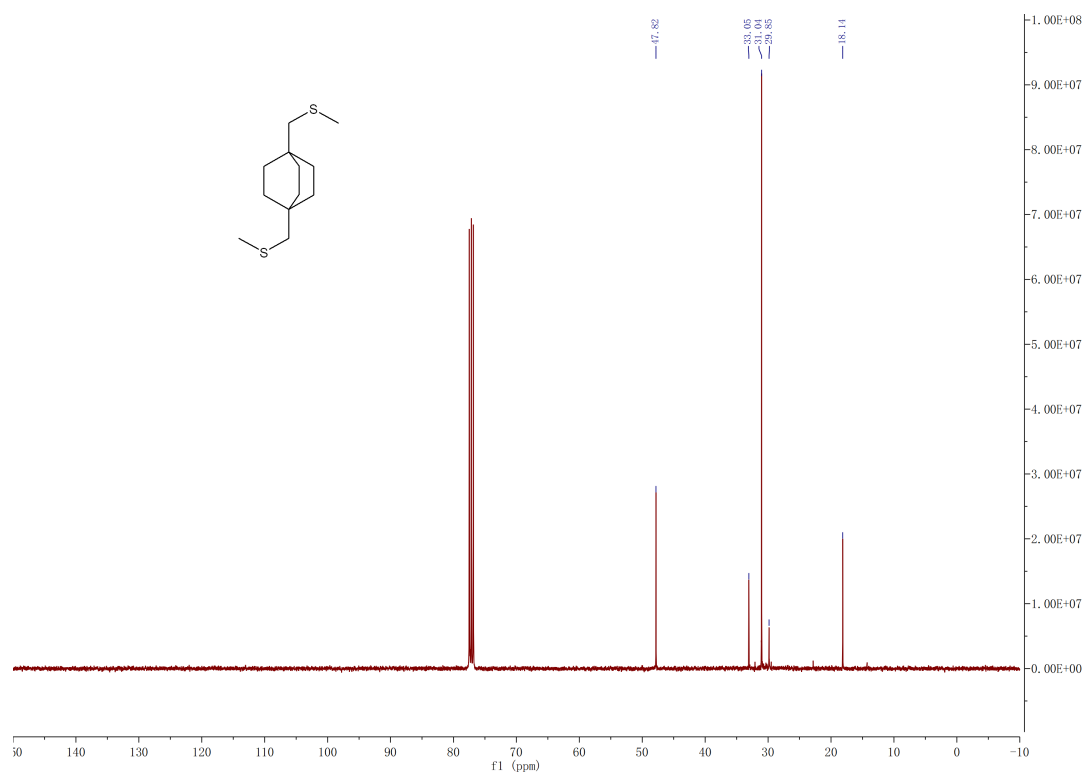
Sodium thiomethoxide (0.741 mmol, 51 mg, 4.00 equiv) was added to a 20 mL scintillation vial equipped with a stir bar and dissolved in dry ethanol (4 mL), then cooled to 0°C . Compound 4 (0.185 mmol, 50 mg, 1.00 equiv) dissolved in 1 mL THF was added to the vial, and the reaction was stirred for 4 hours. The reaction mixture was concentrated *in vacuo*, dissolved in diethyl ether, then filtered over an alumina plug. The solution was concentrated *in vacuo*, then purified via preparatory silica gel thin layer chromatography in 30% dichloromethane in hexanes to yield a mixture of *trans:cis* isomers as a white solid. ^1H NMR (500 MHz, CDCl_3) δ 2.41 (s, 4H), 2.10 (s, 6H), 1.98 – 1.86 (m, 4H), 1.50 – 1.40 (m, 4H), 1.04 – 0.92 (m, 4H).

D. NMR characterization of the compounds

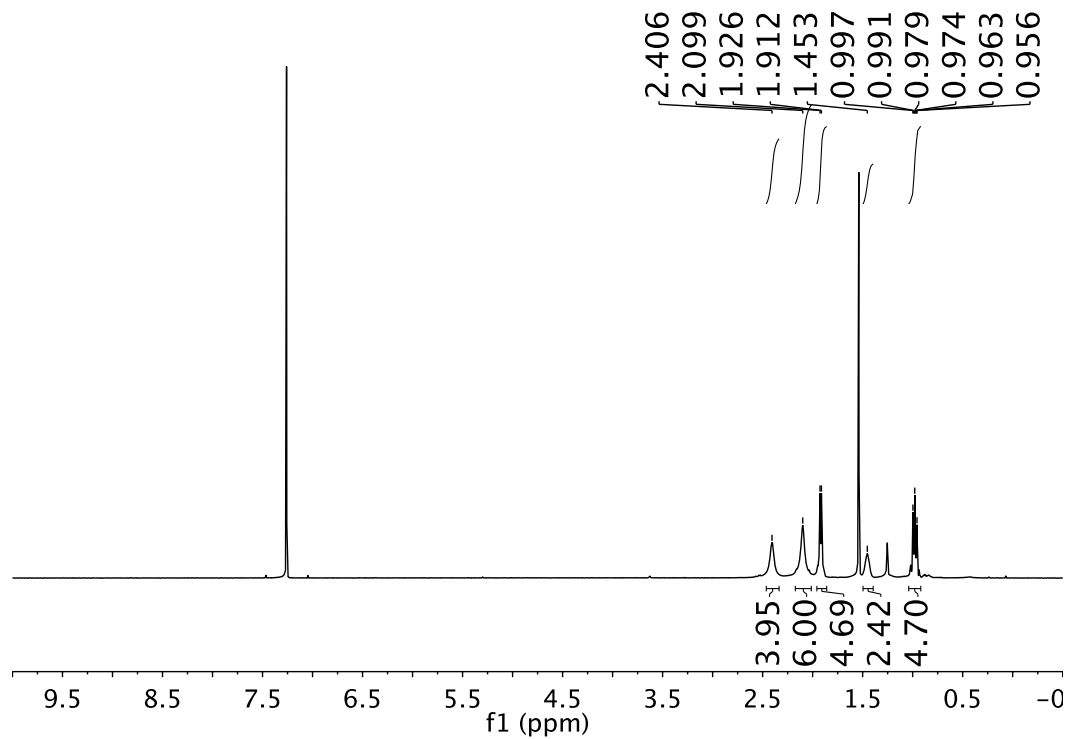
^1H NMR (CDCl_3 , 400 MHz) spectrum of compound **2**.



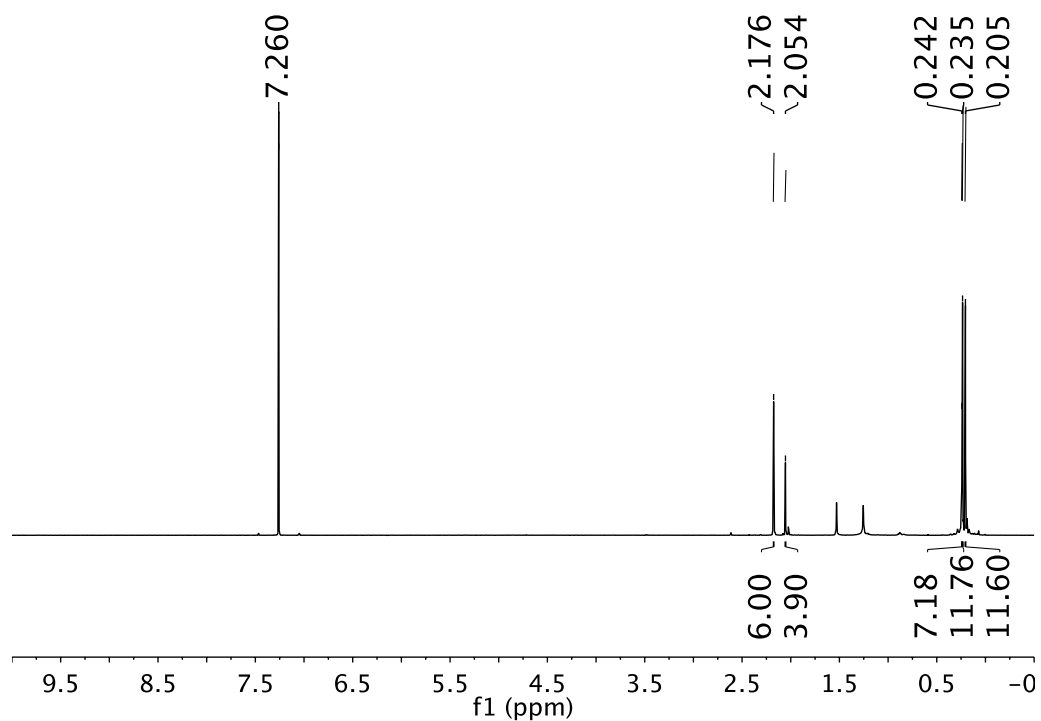
^{13}C NMR (CDCl_3 , 101 MHz) spectrum of compound **2**.



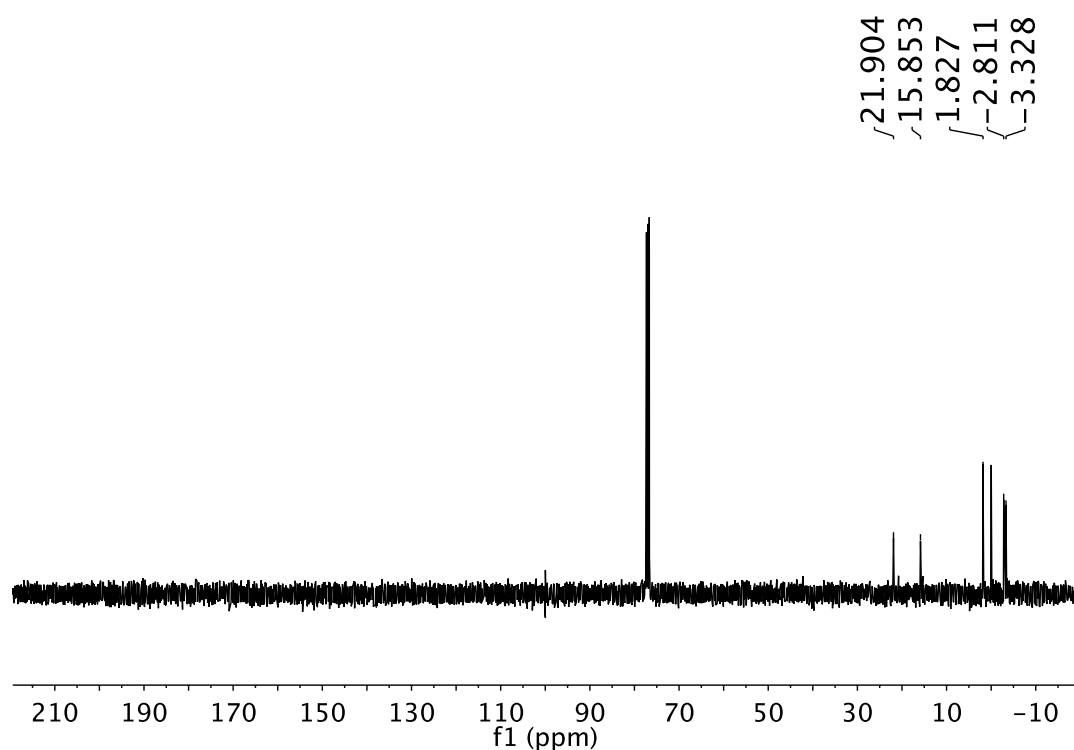
^1H NMR (CDCl_3 , 500 MHz) spectrum of *cyclo-C6(H)*



^1H NMR (CDCl_3 , 500 MHz) spectrum of *cyclo-Si6(Me)*



^{13}C NMR (CDCl_3 , 101 MHz) spectrum of *cyclo-Si6(Me)*



E. Crystal structure of *trans* *cyclo-Si6(Me)*

Data for all compounds was collected on an Agilent SuperNova diffractometer using mirror-monochromated Cu K α or Mo K α radiation. Data collection, integration, scaling (ABSPACK) and absorption correction (face-indexed Gaussian integration²² or numeric analytical methods²³) were performed in CrysAlisPro.²⁴ Structure solution was performed using ShelXS,²⁵ ShelXT,²⁶ or SuperFlip.²⁷ Subsequent refinement was performed by full-matrix least-squares on F2 in ShelXL.²⁵ Olex2²⁸ was used for viewing and to prepare CIF files. PLATON²⁹ was used extensively for SQUEEZE,³⁰ ADDSYM³¹ and TwinRotMat. Many disordered solvent molecules were modeled as rigid fragments from the Idealized Molecular Geometry Library.³² Thermal ellipsoids are rendered at the 50% probability level.

The *trans*-isomer of ***cyclo-Si6(Me)*** was first dissolved in diethyl ether and was slowly evaporated at -30°C. Colorless crystals of ***cyclo-Si6(Me)*** were obtained which were then sent for X-ray diffraction and further analysis. The structure is shown in Figure S8 and available online as cif-file.

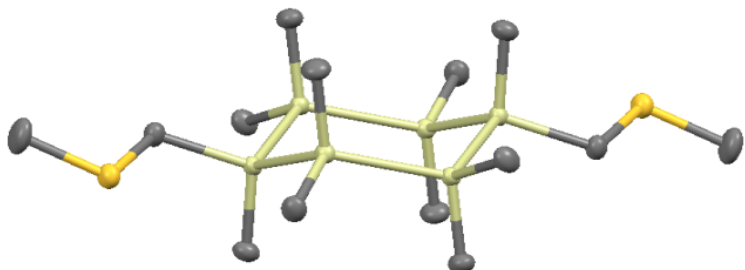


Figure S8. X-ray crystal structure of *trans* *cyclo-Si6(Me)*. Hydrogen atoms are omitted for clarity. Gray: carbon; green: Silicon; Yellow: Sulfur.

F. Molecular orbitals

Molecular orbitals for the cyclic and bicyclic compounds were calculated as described in the manuscript using GPAW¹⁷, and plotted using the standard iso-value of 0.02 using jmol.³³ The orbitals are qualitatively very similar when calculated at the M06-2X/6-311G(d) level of theory.

Plotted in Figure S9 and S10 are the HOMO and HOMO-1. The phase of the non-methylated and permethylated compounds differ systematically. Looking at whether the *p*-components of the orbitals on each of the two sulfur atoms are in or out of phase, the HOMO of the non-methylated have opposite signs and the HOMO-1 have same signs. This trend is reversed in the permethylated compounds; the sulfur components in the HOMO have the same sign, and in the HOMO-1 have opposite signs.

It is clear that the substituents change the character of the HOMO in a way that makes it *switch place* with the HOMO-1. This is known to change if there is an alteration (appearance or removal) of destructive interference in π -conjugated molecules.³⁴

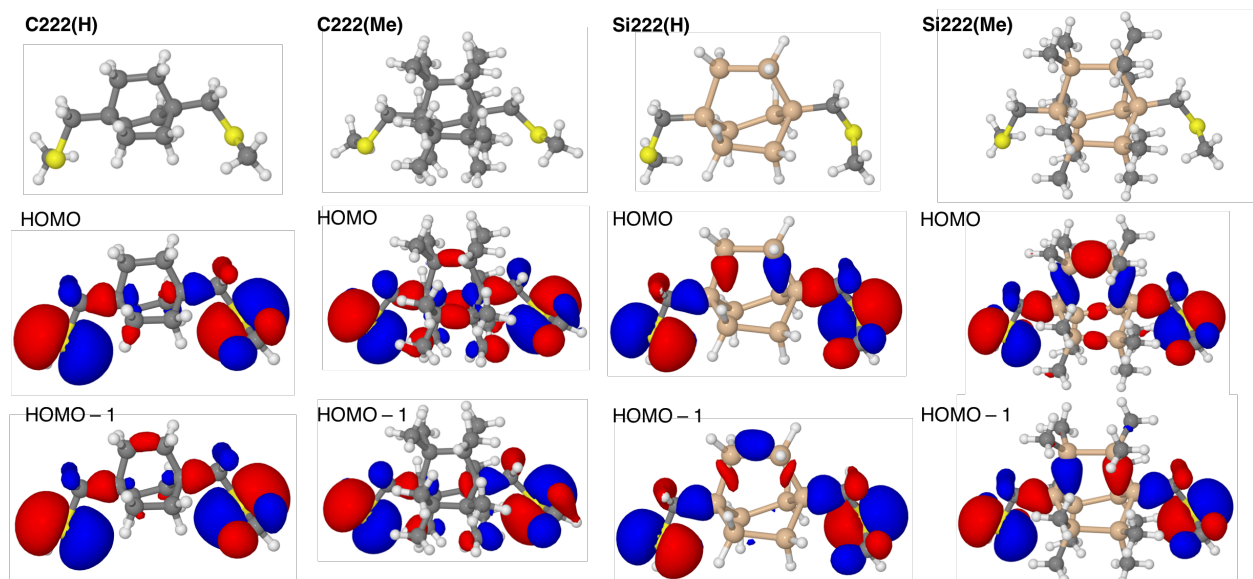


Figure S9. Optimized structures from the junction calculations with plots of HOMO and HOMO-1 of the C222(H), C222(Me), Si222(H), and Si222(Me).

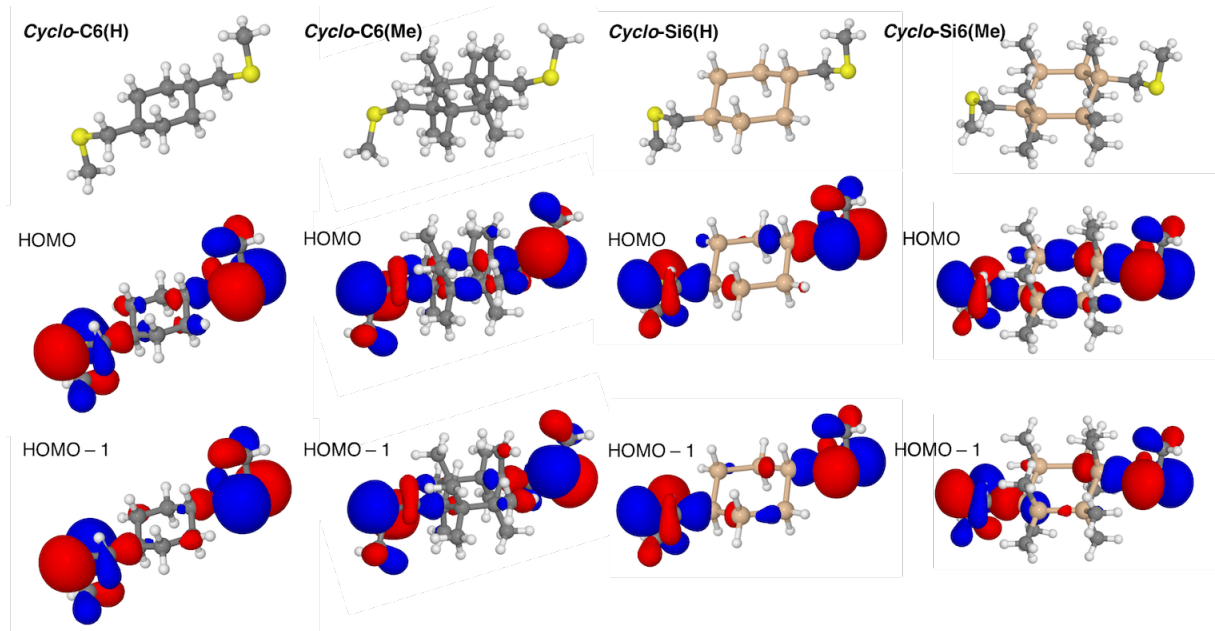


Figure S10. Optimized structures from the junction calculations with plots of HOMO and HOMO-1 of the *cyclo-C6(H)*, *cyclo-C6(Me)*, *cyclo-Si6(H)*, and *cyclo-Si6(Me)*.

In Table S9 the orbital splitting (the energy difference between HOMO and HOMO-1 eigenvalues) are listed calculated at both levels of theory. We note that these are calculated on the optimized junction structures without Au atoms, i.e. these are structures optimized at PBE/DZP level of theory as described in the manuscript. The splittings are of a similar magnitude for the permethylated and non-methylated structures on the order of 0.1 eV (~9.6 kJ/mol, ~2.3 kcal/mol). However, as seen in Figure S9 and S10, the orbitals split in opposite directions for the permethylated and non-methylated compounds.

The splittings are similar at both levels of theory, although somewhat larger at the M06-2X level of theory for the permethylated compounds.

Table S9. Absolute energy difference of HOMO and HOMO-1 eigenvalues given in meV. Note that for both calculations, the isolated molecule is taken from the optimized junction structure at the PBE/DZP level of theory.

	PBE/DZP (GPAW)	M06-2X/6- 311G(d) (Gaussian09)
<i>cyclo</i>-Si6(H)	74	82
<i>cyclo</i>-Si6(Me)	71	129
Si222(H)	27	5
Si222(Me)	62	156
<i>cyclo</i>-C6(H)	95	101
<i>cyclo</i>-C6(Me)	99	152
C222(H)	74	75
C222(Me)	69	126

There is one small exception to the direct agreement between the two levels of theory shown in table S9. For Si222(H) the orbitals are practically not split, and thus the two orbitals are almost fully localized on each sulfur and do not clearly resemble the orbitals shown in Figure S9. If the structure is reoptimized with the M06/2X functional (with the terminal methyl groups in ortho configuration, with the molecule in vacuum) the qualitative agreement is recovered with orbitals visually similar to those in Figure S9, and a splitting of 40 meV (3.9 kJ/mol, 0.9 kcal/mol).

G. Transmission of Linear Molecules

We have calculated the transmission for the series of methylthiomethyl-functionalized linear permethylated (Me) and non-methylated (H) alkanes (C) and silanes (Si). All calculations were carried out as described in the manuscript using GPAW¹⁷ and ATK.¹⁸ Note that for the non-methylated alkane, C(H), the numbering is different from the experimental data in the manuscript to make the numbering-scheme comparable to the other linear systems. All transmission plots are shown in Figure S11, along with the plot of decay as a function of length measured as the sulfur-sulfur distance. In both cases the non-methylated transmission is higher than that of the permethylated system. However, we note that the difference is small between the two alkane series, and for n=3 the transmission is actually higher for the permethylated alkane, as recently presented by Gryn'ova and Corminboeuf.³⁵ We note that, as far as we can tell, none of these results are qualitatively different from theirs. As we have discussed in the manuscript, the general conclusion of our study is, however, different from their work. Future work must help address the complex structure-function relationship of short and oligomeric saturated compounds.

The transmissions of the C(H) and Si(Me) series are used to generate the plot in Figure 2c in the manuscript.

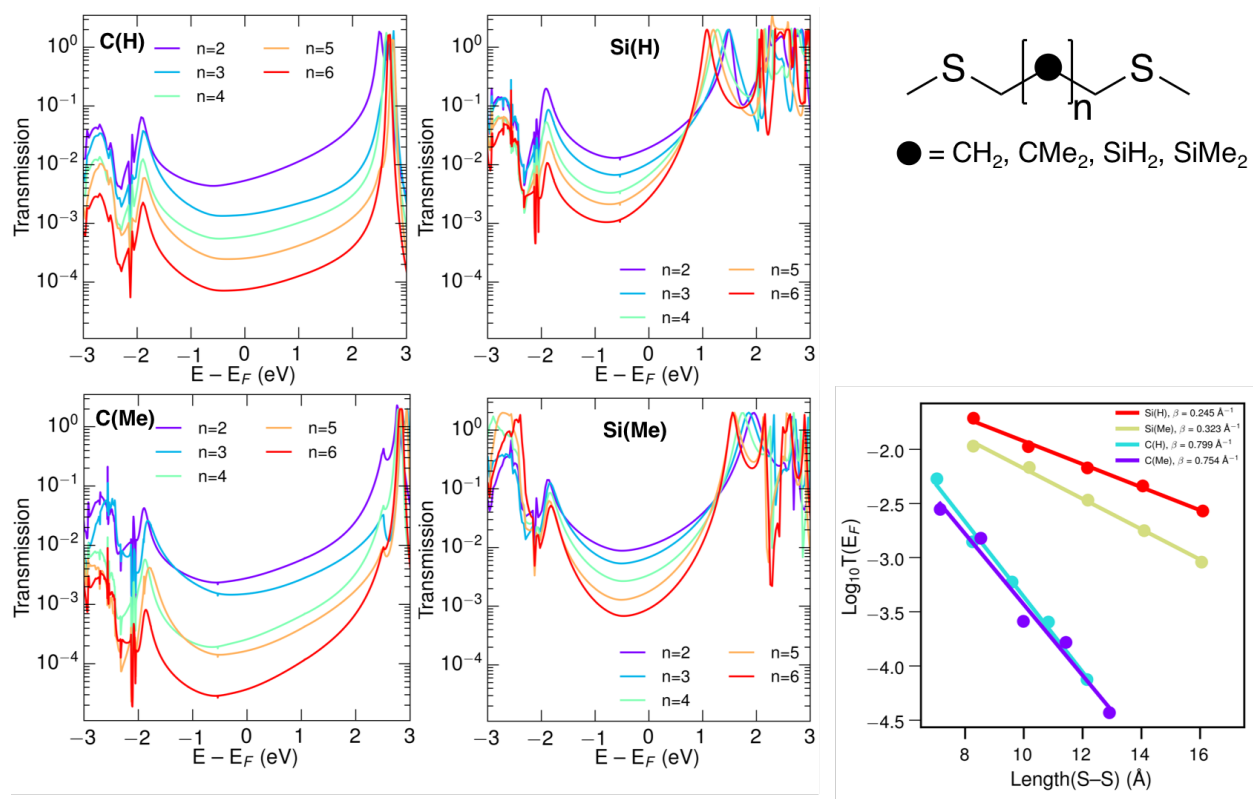


Figure S11. Transmission plots and decay plots of transmission at the Fermi energy with length for the C(H), C(Me), Si(H), and Si(Me) series, with n = 2-6.

REFERENCES

1. Tekautz, G.; Binter, A.; Hassler, K.; Flock, M., Chair, Boat and Twist Conformation of Dodecamethylcyclohexasilane and Undecamethylcyclohexasilane: A Combined DFT and Raman Spectroscopic Study. *ChemPhysChem* **2006**, 7 (2), 421-429.
2. Hölbling, M.; Flock, M.; Hassler, K., The Cyclohexasilanes Si₆H₁₁X and Si₆Me₁₁X with X=F, Cl, Br and I: A Quantum Chemical and Raman Spectroscopic Investigation of a Multiple Conformer Problem. *ChemPhysChem* **2007**, 8 (5), 735-744.
3. Garner, M. H.; Li, H.; Chen, Y.; Su, T. A.; Shangguan, Z.; Paley, D. W.; Liu, T.; Ng, F.; Li, H.; Xiao, S.; Nuckolls, C.; Venkataraman, L.; Solomon, G. C., Comprehensive suppression of single-molecule conductance using destructive σ -interference. *Nature* **2018**, 558 (7710), 415-419.
4. Li, H.; Garner, M. H.; Shangguan, Z.; Chen, Y.; Zheng, Q.; Su, T. A.; Neupane, M.; Liu, T.; Steigerwald, M. L.; Ng, F.; Nuckolls, C.; Xiao, S.; Solomon, G. C.; Venkataraman, L., Large Variations in the Single-Molecule Conductance of Cyclic and Bicyclic Silanes. *J. Am. Chem. Soc.* **2018**, 140 (44), 15080-15088.
5. Perdew, J. P.; Burke, K.; Ernzerhof, M., Generalized Gradient Approximation Made Simple. *Phys. Rev. Lett.* **1996**, 77 (18), 3865-3868.
6. Larsen, A. H.; Mortensen, J. J.; Blomqvist, J.; Castelli, I. E.; Christensen, R.; Dułak, M.; Friis, J.; Groves, M. N.; Hammer, B.; Hargus, C.; Hermes, E. D.; Jennings, P. C.; Jensen, P. B.; Kermode, J.; Kitchin, J. R.; Kolsbjer, E. L.; Kubal, J.; Kaasbjer, K.; Lysgaard, S.; Maronsson, J. B.; Maxson, T.; Olsen, T.; Pastewka, L.; Peterson, A.; Rostgaard, C.; Schiøtz, J.; Schütt, O.; Strange, M.; Thygesen, K. S.; Vegge, T.; Vilhelmsen, L.; Walter, M.; Zeng, Z.; Jacobsen, K. W., The atomic simulation environment—a Python library for working with atoms. *J. Phys.: Condens. Matter* **2017**, 29 (27), 273002.
7. Mortensen, J. J.; Hansen, L. B.; Jacobsen, K. W., Real-space grid implementation of the projector augmented wave method. *Phys. Rev. B* **2005**, 71 (3), 035109.
8. Larsen, A. H.; Vanin, M.; Mortensen, J. J.; Thygesen, K. S.; Jacobsen, K. W., Localized atomic basis set in the projector augmented wave method. *Phys. Rev. B* **2009**, 80 (19), 195112.
9. Zhao, Y.; Truhlar, D. G., The M06 suite of density functionals for main group thermochemistry, thermochemical kinetics, noncovalent interactions, excited states, and transition elements: two new functionals and systematic testing of four M06-class functionals and 12 other functionals. *Theor. Chem. Acc.* **2008**, 120 (1), 215-241.
10. Frisch, M. J.; Trucks, G. W.; Schlegel, H. B.; Scuseria, G. E. Scuseria; Robb, M. A.; Cheeseman, J. R.; Scalmani, G.; Barone, V.; Mennucci, B.; Petersson, G. A.; Nakatsuji, H.; Caricato, M.; Li, X.; Hratchian, H. P.; Izmaylov, A. F.; Bloino, J.; Zheng, G.; Sonnenberg, J. L.; Hada, M.; Ehara, M.; Toyota, K.; Fukuda, R.; Hasegawa, J.; Ishida, M.; Nakajima, T.; Honda, Y.; Kitao, O.; Nakai, H.; Vreven, T.; J. A. Montgomery, J.; Peralta, J. E.; Ogliaro, F.; Bearpark, M.; Heyd, J. J.; Brothers, E.; Kudin, K. N.; Staroverov, V. N.; Keith, T.; Kobayashi, R.; Normand, J.; Raghavachari, K.; Rendell, A.; Burant, C.; Iyengar, S. S.; Tomasi, J.; Cossi, M.; Rega, N.; Millam, J. M.; Klene, M.; Knox, J. E.; Cross, J. B.; Bakken, V.; Adamo, C.; Jaramillo, J.; Gomperts, R.; Stratmann, R. E.; Yazayev, O.; Austin, A. J.; Cammi, R.; Pomelli, C.; Ochterski, J. W.; Martin, R. L.; Morokuma, K.; Zakrzewski, V. G.; Voth, G. A.; Salvador, P.; Dannenberg, J. J.; Dapprich, S.; Daniels, A. D.; Farkas, O.; Foresman, J. B.; Ortiz, J. V.; Cioslowski, J.; Fox, D. J. *Gaussian 09, Rev. D.01*, Gaussian, Inc., Wallingford CT, 2013.: 2013.
11. Leong, M. K.; Mastryukov, V. S.; Boggs, J. E., Structure and Conformations of Six-Membered Systems A₆H₁₂ (A = C, Si): Ab Initio Study of Cyclohexane and Cyclohexasilane. *J. Phys. Chem.* **1994**, 98 (28), 6961-6966.

12. Leventis, N.; Hanna, S. B.; Sotiriou-Leventis, C., A Three-Dimensional Energy Surface for the Conformational Inversion of Cyclohexane. *J. Chem. Educ.* **1997**, *74* (7), 813.
13. Jonsson, H.; Mills, G.; Jacobsen, K. W., *Classical and Quantum Dynamics in Condensed Phase Systems*. World Scientific: 1998.
14. Henkelman, G.; Uberuaga, B. P.; Jónsson, H., A climbing image nudged elastic band method for finding saddle points and minimum energy paths. *J. Chem. Phys.* **2000**, *113* (22), 9901-9904.
15. Smidstrup, S.; Pedersen, A.; Stokbro, K.; Jónsson, H., Improved initial guess for minimum energy path calculations. *J. Chem. Phys.* **2014**, *140* (21), 214106.
16. George, C. B.; Ratner, M. A.; Lambert, J. B., Strong Conductance Variation in Conformationally Constrained Oligosilane Tunnel Junctions. *J. Phys. Chem. A* **2009**, *113* (16), 3876-3880.
17. Enkovaara, J.; Rostgaard, C.; Mortensen, J. J.; Chen, J.; Dułak, M.; Ferrighi, L.; Gavnholt, J.; Glinsvad, C.; Haikola, V.; Hansen, H. A.; Kristoffersen, H. H.; Kuisma, M.; Larsen, A. H.; Lehtovaara, L.; Ljungberg, M.; Lopez-Acevedo, O.; Moses, P. G.; Ojanen, J.; Olsen, T.; Petzold, V.; Romero, N. A.; Stausholm-Møller, J.; Strange, M.; Tritsaris, G. A.; Vanin, M.; Walter, M.; Hammer, B.; Häkkinen, H.; Madsen, G. K. H.; Nieminen, R. M.; Nørskov, J. K.; Puska, M.; Rantala, T. T.; Schiøtz, J.; Thygesen, K. S.; Jacobsen, K. W., Electronic structure calculations with GPAW: a real-space implementation of the projector augmented-wave method. *J. Phys. Condens. Matter* **2010**, *22* (25), 253202.
18. *Virtual NanoLab version 2016.3, Atomistix ToolKit version 2016.3*, QuantumWise A/S (www.quantumwise.com).
19. Garner, M. H.; Koerstz, M.; Jensen, J. H.; Solomon, G. C., The Bicyclo[2.2.2]octane Motif: A Class of Saturated Group 14 Quantum Interference Based Single-Molecule Insulators. *J. Phys. Chem. Lett.* **2018**, *9* (24), 6941-6947.
20. Kumar, K.; Wang, S. S.; Sukenik, C. N., Synthesis, characterization, and chemistry of bridgehead-functionalized bicyclo[2.2.2]octanes: reactions at neopentyl sites. *J. Org. Chem.* **1984**, *49* (4), 665-670.
21. Fischer, R.; Konopa, T.; Ullý, S.; Baumgartner, J.; Marschner, C., Route Si6 revisited. *Journal of Organometallic Chemistry* **2003**, *685* (1), 79-92.
22. Blanc, E.; Schwarzenbach, D.; Flack, H. D., The evaluation of transmission factors and their first derivatives with respect to crystal shape parameters. *J. Appl. Cryst.* **1991**, *24* (6), 1035-1041.
23. Clark, R. C.; Reid, J. S., The analytical calculation of absorption in multifaceted crystals. *Acta Crystallographica Section A* **1995**, *51* (6), 887-897.
24. *O. D. CrysAlisPRO*, Yarnton, England Search PubMed: 2011.
25. Sheldrick, G., A short history of SHELX. *Acta Crystallographica Section A* **2008**, *64* (1), 112-122.
26. Sheldrick, G., Crystal structure refinement with SHELXL. *Acta Crystallographica Section C* **2015**, *71* (1), 3-8.
27. Palatinus, L.; Chapuis, G., SUPERFLIP – a computer program for the solution of crystal structures by charge flipping in arbitrary dimensions. *J. Appl. Cryst.* **2007**, *40* (4), 786-790.
28. Dolomanov, O. V.; Bourhis, L. J.; Gildea, R. J.; Howard, J. A. K.; Puschmann, H., OLEX2: a complete structure solution, refinement and analysis program. *J. Appl. Cryst.* **2009**, *42* (2), 339-341.
29. Spek, A., Structure validation in chemical crystallography. *Acta Crystallographica Section D* **2009**, *65* (2), 148-155.

30. Van Der Sluis, P.; Spek, A. L., BYPASS: an effective method for the refinement of crystal structures containing disordered solvent regions. *Acta Crystallographica Section A* **1990**, *46* (3), 194-201.
31. Le Page, Y., MISSYM1.1 – a flexible new release. *J. Appl. Cryst.* **1988**, *21* (6), 983-984.
32. Guzei, I., An idealized molecular geometry library for refinement of poorly behaved molecular fragments with constraints. *J. Appl. Cryst.* **2014**, *47* (2), 806-809.
33. Jmol: an open-source Java viewer for chemical structures in 3D. <http://www.jmol.org/>.
34. Yoshizawa, K.; Tada, T.; Staykov, A., Orbital Views of the Electron Transport in Molecular Devices. *J. Am. Chem. Soc.* **2008**, *130* (29), 9406-9413.
35. Gryn'ova, G.; Corminboeuf, C., Topology-Driven Single-Molecule Conductance of Carbon Nanowires. *J. Phys. Chem. Lett.* **2019**, *10*, 825-830.